

---

# LEARNING MODAL-MIXED CHAIN-OF-THOUGHT REASONING WITH LATENT EMBEDDINGS

Yifei Shao, Kun Zhou\*, Ziming Xu, Mohammad Atif Quamar†,  
 Shibo Hao, Zhen Wang, Zhiting Hu, Biwei Huang  
 University of California, San Diego

## ABSTRACT

We study how to extend chain-of-thought (CoT) beyond language to better handle multimodal reasoning. While CoT helps LLMs and VLMs articulate intermediate steps, its text-only form often fails on vision-intensive problems where key intermediate states are inherently visual. We introduce modal-mixed CoT, which interleaves textual tokens with compact visual “sketches” represented as latent embeddings. To bridge the modality gap without eroding the original knowledge and capability of the VLM, we use the VLM itself as an encoder and train the language backbone to reconstruct its own intermediate vision embeddings, to guarantee the semantic alignment of the visual latent space. We further attach a diffusion-based latent decoder, invoked by a special control token and conditioned on hidden states from the VLM. In this way, the diffusion head carries fine-grained perceptual details while the VLM specifies high-level intent, which cleanly disentangles roles and reduces the optimization pressure of the VLM. Training proceeds in two stages: supervised fine-tuning on traces that interleave text and latents with a joint next-token and latent-reconstruction objective, followed by reinforcement learning that teaches when to switch modalities and how to compose long reasoning chains. Extensive experiments across 11 diverse multimodal reasoning tasks, demonstrate that our method yields better performance than language-only and other CoT methods. Our code will be publicly released.

## 1 INTRODUCTION

Chain-of-thought (CoT) (Wei et al., 2022; Zhou et al., 2022) has enabled large language models (LLMs) and vision-language models (VLMs) to generate intermediate reasoning steps and substantially improve performance on complex tasks (Chen et al., 2023; Zhang et al., 2024). By encouraging models to articulate stepwise deductions, CoT can better elicit LLMs and VLMs to generate accurate and faithful responses. However, its language-only form struggles on multimodal problems (*e.g.*, 3D spatial reasoning and visually grounded logical queries (Zhu et al., 2024)), where crucial intermediate states are inherently *visual* rather than textual. Many multimodal tasks require mental rotation and transforms, or fine-grained spatial relations that are cumbersome to describe in words. These limitations become more acute under vision-intensive and long-horizon spatio-temporal dependencies, where purely verbal descriptions fail to capture evolving visual context (Gao et al., 2025).

Humans address these cases by engaging *mental imagery* (Pylyshyn, 2002; Richardson, 2013): we sketch, reposition, and manipulate latent visuals in mind, externalizing only the pieces that matter for multi-hop reasoning (Yang et al., 2025b). Cognitive studies describe a visuospatial “sketchpad” that complements verbal working memory, enabling rapid simulation of object poses, trajectories, and constraints with minimal verbalization. This latent, modality-interleaved process lets us flexibly switch between words and pictures, preserving speed while maintaining grounding. Motivated by this paradigm, we seek to equip VLMs with *modal-mixed* CoT: the ability to interleave textual tokens with compact visual “sketches” represented as latent embeddings. Such embeddings act as lightweight, model-native carriers of visual state, allowing the reasoning process to offload visual details to condensed latent embeddings while reserving language for high-level logic control. In

---

\*Corresponding author: kuzhou@ucsd.edu

†Work done during an internship at UCSD.

---

doing so, we aim to reason beyond what text can describe, improve grounding, and make complex vision-intensive reasoning tasks both more accurate and more efficient.

A central challenge is the modality gap: inserting a new visual generation pathway must not erode the VLM’s original linguistic knowledge and capabilities (Yi et al., 2025). Therefore, we should guarantee that the visual latent space is both *aligned* with the VLM’s internal representations and *predictable* from its outputs. First, inspired by recent VLM-as-encoder ideas (Yang et al., 2025b; Wu et al., 2025), we use the visual encoder and connection layer from the VLM itself as the latent embedding encoder. Specifically, we train the VLM to reconstruct its visual encoder produced embeddings for intermediate images within the modal-mixed chain-of-thought. In this way, the generated latent visual “rationales” will be in the same semantic space as its native features. This alignment makes the latent embeddings easy for the VLM to generate and consume. Second, we attach a diffusion-based latent decoder that is triggered by a special *start* token and conditioned on the VLM’s hidden states to produce continuous visual embeddings. Benefiting from the strong vision generation ability, the diffusion model is able to carry the burden of fine-grained perceptual details, while the VLM focuses on supplying compact, high-level intent. Such a disentanglement-based design simplifies the function of the VLM and eases its learning objective, reducing the risk of catastrophic forgetting caused by overfitting visual details.

Building on these components, we adopt a two-stage training strategy for modal-mixed CoT. We first perform supervised fine-tuning on curated traces that interleave text and latent visuals to teach the format and basic skills. The objective couples next-token prediction with latent reconstruction, so the model learns *what* to sketch and *how* to reference those sketches later. Then, we apply reinforcement learning on the VLM to learn *when* to switch modalities and *how* to compose textual and latent steps for complex problems. Extensive experiments across 11 multimodal tasks demonstrate consistent gains over language-only CoT and strong improvements on complex visual reasoning tasks.

We summarize the key contribution of this paper as:

- We devise an architecture that integrates VLM with a diffusion model based decoder, to support modal-mixed reasoning with latent visual embeddings.
- We leverage a two-stage training strategy that first learns the modal-interleaved reasoning paradigm via supervised fine-tuning, then reinforcement learning for further adapt the two modes.
- Extensive experiments on 11 multimodal tasks have shown the effectiveness of our approach.

## 2 RELATED WORK

**Vision-language Models.** VLMs are adapted to interpret visual information to understand multimodal documents, forms, and charts where text and images are intertwined. Modern VLMs typically adopt a three-component architecture consisting of a vision encoder, a foundational LLM, and a connector module. Pioneering models such as Flamingo (Alayrac et al., 2022), BLIP (Li et al., 2023), and LLaVA (Liu et al., 2023a) were instrumental in establishing this paradigm for tasks like image captioning and visual question answering. Recent works have focused on refining the training process. A surge of work scales up the training data of VLMs and observes the improved performance on the reasoning ability, *e.g.*, KOSMOS-2 (Peng et al., 2023), InternVL2.5 (Chen et al., 2024b), and Qwen2.5VL (Bai et al., 2025b). In addition, advanced post-training techniques like visual instruction tuning (Liu et al., 2023b) and reinforcement learning (Chen et al., 2025c) have also been applied in VLM to enhance the task solving capabilities. However, since VLMs can only generate language-based rationales, they do not perform well on vision-intensive tasks, *e.g.*, spatial and multi-image reasoning (Chen et al., 2025a). Although recent works have proposed unified generative models that can produce either text or vision outputs, their benchmark performance is still not as better as state-of-the-art VLMs (Wang et al., 2025b). In this paper, we adapt a VLM into a multimodal reasoner that can perform interleaved reasoning in vision and text modals. We simplify the vision generation task into producing high-level visual latent embeddings.

**Chain-of-thought Reasoning.** Chain-of-thought (CoT) reasoning has been widely explored as a way to enhance LLM performance by explicitly generating intermediate reasoning traces before producing final predictions (Wei et al., 2022; Khot et al., 2022; Zhou et al., 2022; Yue et al., 2023; Yu et al., 2023; Wang et al., 2024; Havrilla et al., 2024). Recent advances show that large-scale

RL training can encourage models to generate much longer CoT and achieve stronger performance through test-time scaling, as demonstrated by OpenAI O1 (Jaech et al., 2024) and DeepSeek R1 (Guo et al., 2025). Beyond simple linear chains, researchers have extended CoT into tree-structured reasoning paradigms (Yao et al., 2023; Xie et al., 2023; Hao et al., 2024a). CoT methods are also widely used in VLMs for solving multimodal reasoning tasks (Zhang et al., 2024). Recent works have proposed to use interleaved CoT for solving vision-intensive tasks (Gao et al., 2025). By equipping with visual tools (*e.g.*, zooming in and drawing lines), VLMs can learn to interleave the tool use and text generation, to edit the input for composing intermediate image to guide reasoning (Wang et al., 2025a). However, such a way cannot handle open questions that might require special operations on the images (*e.g.*, drawing irregular masks). To solve it, we aim to internalize the image generation process into producing latent visual embeddings, which enable the VLM to learn generating high-level semantics and also reduce the inference latency from tool invocation.

**Latent Reasoning.** Another line of recent works investigates latent reasoning, where the reasoning process happens in hidden states rather than being explicitly generated in language. Methods such as introducing special latent tokens (Goyal et al., 2023; Pfau et al., 2024), knowledge distillation (Deng et al., 2023; 2024; Yu et al., 2024), or architectural modifications (Giannou et al., 2023; Fan et al., 2024; Barrault et al., 2024) aim to strengthen this capability by improving the expressivity of the transformer network and designing new supervision methods. Continuous CoT (Hao et al., 2024b; Zhu et al., 2025) replaces language-based CoT with continuous embeddings. It demonstrates that reasoning in latent space can break free from the constraint of discrete language tokens, allowing the model to encode superpositions of search paths in parallel and yielding efficiency gains. MVoT (Li et al., 2025b) trains a unified model to directly produce images and actions in interleaving trajectories. Recently, Mirage (Yang et al., 2025b) proposes to empower VLM with latent visual tokens for multimodal reasoning, which uses the visual encoder of VLM for supervised fine-tuning using cosine similarity loss. In this work, we follow it and optimize the architecture by using diffusion decoder.

### 3 PRELIMINARY

**Vision Language Models.** VLMs extend a large language model (LLM) with visual perception so the model can “read” images as part of its context (Chen et al., 2024a). A standard VLM has three parts: (i) a vision encoder (*e.g.*, a ViT (Dosovitskiy et al., 2020)) that maps an input image to a sequence of visual features; (ii) a connector that projects these visual features into LLM-compatible “visual tokens”, *i.e.*, continuous embeddings placed where tokens would appear; and (iii) the LLM backbone, which consumes a mixed sequence of visual and text tokens to produce a textual response. Given an image  $I$  and text instruction  $q$ , the encoder yields features  $\phi_v(I)$ ; the connector  $g$  produces visual embeddings  $\mathbf{z} = g(\phi_v(I))$ ; the LLM then attends over the concatenated sequence  $[\mathbf{z}, q]$  and autoregressively generates an answer  $y$ . Training uses the standard next-token objective on a multimodal sequence  $x = \{x_1, \dots, x_n\}$ , where each  $x_i$  is a discrete text token:

$$P_\theta(x_{1:n}) = \prod_{i=1}^n P_\theta(x_i | x_{<i}, \mathbf{z}), \quad \mathcal{L}(\theta) = - \sum_{i=1}^n \log P_\theta(x_i | x_{<i}, \mathbf{z}), \quad (1)$$

so the model learns to predict each next token based on both linguistic context and visual evidence.

**Chain-of-thought.** CoT prompting is a widely used tactic for LLMs and VLMs to produce step-by-step solutions that make hard reasoning tasks easier. It works because the model is asked to externalize rationales (*i.e.*, short, structured intermediate steps), which organize relevant facts from the prompt, reduce search complexity, and keep the attention on task-critical context. In this way, CoT first generates a sequence of textual rationales and then an answer, denoted as  $\{x_1, \dots, x_n, a\}$ .

In our setting, we extend CoT to modal-mixed CoT, where the reasoning trace interleaves natural-language tokens with compact latent visual embeddings. The model autoregressively generates the trace as  $\{x_1, z_1, \dots, z_n, x_n, a\}$ . In this way, textual steps can invoke or reference latent visual states when helpful, enabling grounded, efficient multimodal reasoning.

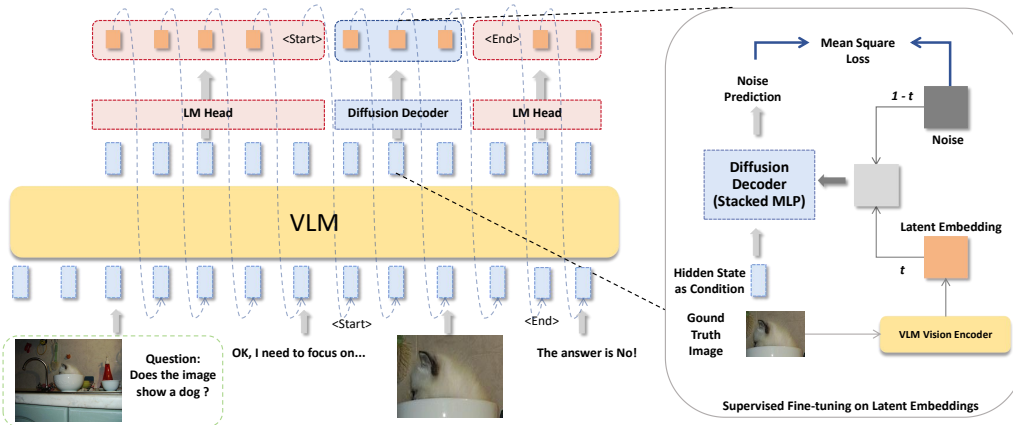


Figure 1: The overview of our proposed method. We integrate the diffusion model based decoder into the VLM and train it to learn the interleaved modal-mixed CoT reasoning paradigm.

## 4 APPROACH

We propose the modal-mixed chain-of-thought reasoning method that can interleave text tokens and visual latent embeddings, for solving vision-intensive complex tasks. To achieve it, we modify the original architecture of the VLM to support the new reasoning paradigm, and devise the fine-tuning strategy for learning it. The overview of the proposed method is shown in Figure 1.

### 4.1 MODEL ARCHITECTURE

Based on the original VLM architecture, we integrate it with a diffusion model based decoder (Yang et al., 2025b) for generating latent visual embeddings, and add special tokens for performing modal-mixed chain-of-thought reasoning during inference.

**Diffusion Model based Decoder.** Inspired by diffusion models in vision generation (Rombach et al., 2022), we employ a conditional diffusion decoder to synthesize the latent visual embeddings that appear inside the modal-mixed CoT. Our design cleanly splits roles: the LLM produces high-level semantic intent, while a lightweight stacked-MLP diffusion network reconstructs fine-grained visual details conditioned on that intent. Concretely, the last-layer hidden state of the LLM serves as the conditioning vector for a token-wise diffusion process that transforms Gaussian noise into a latent embedding. Let  $\mathbf{h}_k$  be the LLM’s final hidden state when generating the  $k$ -th latent step; we map it to a conditioning vector  $\mathbf{c}_k = \mathbf{W}\mathbf{h}_k$ . Starting from  $\mathbf{z}_k^{(T)} \sim \mathcal{N}(0, I)$ , the decoder performs  $T$  denoising steps using a small MLP predictor  $\epsilon_\phi(\cdot)$  (with timestep and condition embeddings) to remove noise:

$$\mathbf{z}_k^{(t-1)} = \frac{1}{\sqrt{\alpha}} \left( \mathbf{z}_k^{(t)} - \frac{1 - \alpha_t}{\sqrt{1 - \bar{\alpha}_t}} \epsilon_\phi(\mathbf{z}_k^{(t)}, t, \mathbf{c}_k) \right) + \sigma_t \xi, \quad \xi \sim \mathcal{N}(0, I), \quad (2)$$

and outputs the latent embedding  $\mathbf{e}_k = \mathbf{z}_k^{(0)}$ . To better adapt with the autoregressive language generation process, we emit these latents autoregressively. Specifically, after producing  $\mathbf{e}_k$ , we feed  $\{\mathbf{e}_1, \dots, \mathbf{e}_k\}$  back into the VLM to obtain the next condition  $\mathbf{c}_{k+1}$ , and repeat the diffusion loop to generate  $\mathbf{e}_{k+1}$ . Such a way unifies the generation paradigm of text tokens and latent embeddings in a next token/latent prediction manner, enabling joint optimization during training.

**Modal-mixed Chain-of-thought Reasoning.** Built on the diffusion decoder, our model performs modal-mixed CoT at inference by interleaving text tokens with latent visual embeddings. We introduce two special vocabulary items:  $\langle \text{START} \rangle$  and  $\langle \text{END} \rangle$ , with randomly initialized embeddings. When generated, they switch the decoder between the standard language head and the diffusion latent head. Specifically, generation begins in the usual text mode; upon emitting  $\langle \text{START} \rangle$ , the model

invokes the diffusion decoder to autoregressively produce a fixed number  $K$  latent embeddings, then appends  $\langle \text{END} \rangle$  and resumes text reasoning. A typical trajectory thus takes the form:

$$[\text{BOS}]; x_{1:i}; \langle \text{START} \rangle; \mathbf{z}_{1:K}; \langle \text{END} \rangle; x_{i+1:j} \cdots [\text{EOS}], \quad (3)$$

This scheme lets the model determine when to sketch, to help text and visuals mutually inform one another. During generation, text specifies what to sketch, and the latent visual embeddings refine and ground subsequent textual reasoning, to help text reasoning search the final answer.

## 4.2 LEARNING TO REASON WITH LATENT EMBEDDINGS

To enable the VLM to perform modal-mixed chain-of-thought reasoning, we employ a two-stage training strategy. First, we adopt supervised finetuning (SFT) to teach the model for learning the interleaved styled reasoning paradigm. Then, we apply reinforcement learning (RL) that can learn its generated modal-mixed CoTs, to further enhance its robustness and generalization capabilities.

**Supervised Fine-tuning with VLM as Visual Latent Encoder.** We first fine-tune the VLM on annotated, modal-interleaved CoT traces in which text rationales alternate with helpful intermediate images. For every intermediate image  $\mathcal{I}$  in a trace, we reuse the VLM’s own vision encoder and connection layer to convert it into dense visual token embeddings denoted as  $\mathbf{V} = g(\phi_v(\mathcal{I})) \in \mathbb{R}^{N \times d}$ . To reduce the context length while preserving high-level semantics, we compress  $\mathbf{V}$  into a fixed-length latent sketch  $\mathbf{z} \in \mathbb{R}^{M \times d}$  through the average pooling operation.

During training, the targeted sequence interleaves text tokens and compressed latent embeddings delimited by  $\langle \text{START} \rangle$  and  $\langle \text{END} \rangle$ . We apply a joint autoregressive (AR) objective, where (i) the language head predicts the next text token; (ii) the diffusion decoder predicts the next latent embedding within the current latent block, conditioned on the VLM hidden state. For text positions  $\mathcal{T}$  we minimize cross-entropy, and for each latent block  $\mathbf{Z} = [\mathbf{z}_1, \dots, \mathbf{z}_M]$ , we sample  $\epsilon \sim \mathcal{N}(\mathbf{0}, \mathbf{I})$  and timestep  $t$ , form  $\mathbf{z}_k^{(t)} = \alpha_t \mathbf{z}_k + \sigma_t \epsilon$ , and regress the diffusion decoder’s velocity prediction  $D_\phi(\mathbf{z}_k^{(t)}, t, \mathbf{c}_k)$  to  $\epsilon$ . The joint loss is formulated as:

$$\mathcal{L} = -\sum_{t \in \mathcal{T}} \log p_\theta(y_t | x, y_{<t}, \mathbf{Z}_{\leq t}) + \lambda \sum_{k=1}^M \|D_\phi(\mathbf{z}_k^{(t)}, t, \mathbf{c}_k) - \epsilon\|_2^2 \quad (4)$$

where  $\lambda$  balances textual next-token prediction and latent diffusion supervision.

**Reinforcement Learning for Self-adaptation.** Supervised fine-tuning (SFT) teaches the model to follow annotated, interleaved CoT traces. However, the provided intermediate images are not guaranteed to be the most helpful for textual reasoning, nor is the textual rationale necessarily ideal for guiding image (latent) generation. To better couple the two modalities, we add a reinforcement learning (RL) phase that lets the model roll out its own modal-mixed CoT and learn to prefer traces where text and latent sketches are mutually supportive. We adopt GRPO (Shao et al., 2024): for each query  $q$ , we sample a group of interleaved outputs  $\{o_i\}_{i=1}^G$  from the current policy  $\pi_{\theta_{\text{old}}}$ , score each with a task accuracy reward  $r_i$ . For rewarding, we test the answer exactly matching accuracy, and assign 1 reward for correct ones and 0 for incorrect ones.

$$\max_{\theta} \mathbb{E} \left[ \frac{1}{G} \sum_{i=1}^G \min(\rho_i A_i, \text{clip}(\rho_i, 1 - \varepsilon, 1 + \varepsilon) A_i) \right], \quad (5)$$

where  $\rho_i = \frac{\pi_\theta(o_i|q)}{\pi_{\theta_{\text{old}}}(o_i|q)}$  and  $A_i = \frac{r_i - \text{mean}(\{r_j\})}{\text{std}(\{r_j\})}$ . We perform RL until convergence, which leads the VLM to discover modal-interleavings where latent visual reasoning genuinely aids the textual chain (and vice versa), yielding a self-adapted, tightly integrated modal-mixed CoT policy. To guarantee the training stability in RL, we do not backpropagate the loss from the latent visual embeddings, and only compute the loss on text tokens.

Model	VCog-Bench		LogicVista		MM-IQ			Average
	CVR	Raven	Ind.	Spat.	Math	Log.	2D.	
<b>Qwen2.5-VL-7B-Instruct</b>	39.8	12.1	25.2	19.0	24.5	24.4	<u>25.2</u>	24.3
<b>LLaVA-OneVision-Qwen2-7B</b>	36.7	<u>13.0</u>	20.6	25.3	<b>29.1</b>	23.5	25.0	24.7
<b>InternVL2.5-8B</b>	38.2	12.3	25.2	19.0	22.1	22.4	21.1	22.9
<b>Janus-Pro-7B</b>	34.5	12.5	20.4	<u>27.9</u>	26.5	19.6	22.7	23.4
<b>R1-onevision-RL</b>	23.3	<b>23.4</b>	29.0	17.7	22.1	22.4	21.1	22.7
<b>MM-EurekaQwen-7B</b>	33.3	10.4	<b>34.6</b>	22.8	25.1	23.7	24.9	25.0
<b>Thyme</b>	32.3	10.8	<u>33.6</u>	19.0	24.1	20.6	23.0	23.3
<b>Ours (SFT)</b>	<u>40.8</u>	11.3	28.0	<b>31.6</b>	<u>27.4</u>	<u>24.6</u>	23.0	<b>26.7</b>
<b>Ours (RL)</b>	<b>42.4</b>	12.1	21.5	25.3	26.3	<b>25.9</b>	<b>26.5</b>	<u>25.7</u>

Table 1: Experimental Results on Vision-intensive Reasoning Task across VCog-Bench, LogicVista, and MM-IQ. Ind. Spat. Log. and 2D. denote inductive reasoning, spatial reasoning, logical operation, and 2D geometry, respectively. We also report the average result across all dimensions. The best and second best methods are marked by bold and underline, respectively.

Model	V* Benchmark		MME-Unify		Average
	Attr	Spatial	Spot Diff.	Aux. Lines	
<b>Qwen2.5-VL-7B-Instruct</b>	72.2	77.6	13.0	32.7	48.8
<b>LLaVA-OneVision-Qwen2-7B</b>	60.0	67.1	27.0	<b>46.2</b>	50.0
<b>InternVL2.5-8B</b>	66.1	69.7	<b>30.0</b>	32.7	49.6
<b>Janus-Pro-7B</b>	–	–	<u>29.0</u>	28.8	–
<b>R1-onevision-RL</b>	77.4	<b>94.5</b>	14.0	30.8	54.2
<b>MM-EurekaQwen-7B</b>	41.7	64.5	19.0	<u>44.2</u>	42.4
<b>Thyme</b>	<b>82.5</b>	78.9	21.0	<b>46.2</b>	<b>57.2</b>
<b>Ours (SFT)</b>	<u>80.2</u>	<u>78.9</u>	27.0	34.6	<u>55.2</u>
<b>Ours (RL)</b>	<u>77.8</u>	<u>76.3</u>	28.0	38.5	55.1

Table 2: Experimental Results on Vision-Intensive Perception Tasks. Spot Diff. and Aux. Lines are the abbreviation of the spot difference and auxiliary lines dimensions, respectively. Note that for VLMs in V\* benchmark all use tools to help them achieve this good performance. The best and second-best methods are marked by bold and underline, respectively.

## 5 EXPERIMENTS

### 5.1 EXPERIMENTAL SETUP

**Evaluation Settings.** We evaluate our model from two perspectives: *vision-intensive perception* and *vision-intensive reasoning*. We select relevant perception and reasoning tasks from existing benchmarks to compose the evaluation datasets, which typically require multi-round derivation on the vision input to reach the answer. For vision-intensive perception, we adopt the visual search benchmark  $V^*$  (Wu & Xie, 2024), which is designed to rigorously assess fine-grained visual analysis under challenging conditions. Unlike conventional models that rely on external zoom-in functions, our model can directly perform intrinsic visual search. We further include perception subtasks from MME-Unify (Xie et al., 2025), a comprehensive benchmark for unified models. We focus on two subtasks: *Spot Difference* requiring localization of subtle differences between paired images, and *Auxiliary Lines* involving geometric guideline drawing and associated numerical reasoning. For vision-intensive reasoning, we employ three representative benchmarks. VCog-Bench (Cao et al., 2024) targets zero-shot abstract visual reasoning (AVR); we select two subsets: CVR, an outlier detection task over compositional visual patterns, and RAVEN (Zhang et al., 2019), an IQ-style matrix reasoning task for abstract rule induction and pattern completion. LogicVista (Xiao et al., 2024) evaluates visual logical reasoning by integrating perception with formal logic; we use the *Inductive* and *Spatial* subsets to assess abstract and visuospatial reasoning. Finally, MM-IQ (Cai et al., 2025) is

---

inspired by human IQ tests and measures multimodal intelligence. We select the three largest and most representative subtasks—*Mathematical*, *2D Geometry*, and *Logical Operation*, which jointly cover numerical problem-solving, geometric reasoning, and symbolic logic, thereby providing a broad evaluation of multimodal reasoning capacity.

**Baseline Methods.** We compare our method against a comprehensive suite of vision-language models categorized by their architectural paradigms and reasoning capabilities. First, we include standard VLMs that couple a vision encoder with an LLM via a connector, specifically Qwen2.5-VL-7B-Instruct (Bai et al., 2025b), LLaVA-OneVision-Qwen2-7B (Liu et al., 2024), and InternVL2.5-8B (Chen et al., 2024b). These models represent the current state-of-the-art in general multimodal understanding through large-scale visual instruction tuning. To evaluate the impact of advanced post-training, we further incorporate reasoning-enhanced models that utilize reinforcement learning (RL) to optimize pure-text Chain-of-Thought (CoT) for complex tasks, namely MM-EurekaQwen-7B (Meng et al., 2025) and R1-onevision-RL (Yang et al., 2025a). Additionally, we compare with models that extend beyond standard text outputs, such as Janus-Pro-7B (Chen et al., 2025b), a unified framework for interleaved image understanding and generation, and Thyme (Zhang et al., 2025), a variant based on Qwen2.5-VL-7B-Instruct that performs visual reasoning by generating executable Python code to invoke external tools. In contrast to these paradigms, our model produces compact visual imagery tokens that act as lightweight visual sketches to facilitate internal reasoning without relying on heavy external processes. Finally, we report results for our own models: Ours (SFT), which reflects gains from instruction-following data, and Ours (RL), which leverages preference optimization to further improve reasoning robustness and output quality.

**Implementation Details.** In this work, we adopt Qwen2.5-VL-7B-Instruct as our base model and perform SFT using Zebra-CoT (Li et al., 2025a), a diverse large-scale dataset containing logically coherent interleaved text-image reasoning traces. Specifically, all images in Zebra-CoT are first resized to  $448 \times 448$  and then passed through the vision encoder, producing 256 latent tokens per image, which are further compressed to 32 via average pooling. To enable the model to transition between text and latent reasoning, we introduce a loss term at the  $\langle \text{START} \rangle$  token. Since latent reasoning bypasses the language modeling head and cannot be directly detokenized, we insert a  $\langle \text{PAD} \rangle$  placeholder whenever latent tokens are generated, in order to facilitate visualization. During training, we freeze the visual encoder and employ different learning rates for different components: the LLM uses a learning rate of  $1e-5$ , while the diffusion head uses a learning rate of  $2e-4$ , in order to achieve better convergence. We further adopt a cosine learning rate scheduler to stabilize optimization. For efficiency, instead of using the entire dataset, we select five representative subcategories, *i.e.*, Visual Jigsaw, Visual Search, Ciphers, RPM, and Tetris, resulting in 71,488 training samples. For RL, we leverage VisuLogic (Xu et al., 2025) as the training data and deduplicate it with the test data. It contains human-verified 1,000 high-quality visual reasoning problems across six categories. The sampling number is set to 500 per instance, and the learning rate is  $5e-6$ .

## 5.2 MAIN RESULTS

Table 1 presents the results on vision-intensive reasoning tasks, where our method (both SFT and RL versions) consistently outperforms or remains highly competitive with other baselines. As shown, standard VLMs like Qwen2.5-VL-7B-Instruct and LLaVA-OneVision-Qwen2-7B generally surpass unified models like Janus-Pro-7B, indicating that large-scale pre-training provides a superior foundation for logical reasoning. However, a critical bottleneck remains even for reasoning-enhanced models derived from these strong backbones, such as R1-onevision-RL and MM-EurekaQwen-7B. Since these models rely purely on text-only CoT, they are constrained by a single static encoding of the input image, which prevents them from reinterpreting visual information or simulating geometric transformations. On the other hand, Thyme is restricted to tool-based pixel edits and cannot represent hypothetical future states, while Janus-Pro-7B, despite its generative capabilities, lacks a disentangling design, causing it to focus on visual details rather than modal-mixed reasoning. In contrast, our model bridges this gap by generating intermediate latent visual states interleaved with text tokens. This latent CoT naturally leverages spatial and perceptual information to “imagine” outcomes that do not exist in the input, while our disentanglement-based design—enabled by a lightweight diffusion decoder—liberates the reasoning process from pixel-level distractions. This allows for

Model	V* Benchmark		MME-Unify		LogicVista		Average
	Attr	Spatial	Spot Diff.	Aux. Lines	Ind.	Spat.	
<b>Ours (SFT)</b>	<b>80.2</b>	<b>78.9</b>	<b>27.0</b>	<b>34.6</b>	<b>28.0</b>	<b>31.6</b>	<b>46.7</b>
- Text-only Training	77.6	71.1	21.0	26.9	21.5	25.3	40.6
- Similarity Loss	<b>81.0</b>	76.3	<b>28.0</b>	<u>32.7</u>	<b>29.9</b>	20.3	44.7
<b>Qwen2.5-VL-7B-Instruct</b>	72.2	<u>77.6</u>	13.0	<u>32.7</u>	25.2	19.0	40.0

Table 3: Ablation study results for text-only training and similarity loss.

the decomposition of complex problems into manageable steps, leading to a much deeper and more effective level of reasoning.

Table 2 presents the results of vision-intensive perception tasks. For the V\* benchmark, all the VLMs here use the zoom-in tools rely on external tools to obtain zoom-in views of local regions as auxiliary inputs, for helping achieve the good performance. Similar to reasoning tasks, Qwen2.5-VL-7B-Instruct exhibits better performance than other baselines, owing to its large-scale training on massive multimodal data. Janus-Pro-7B also demonstrates strong performance on the spot difference task of MME-Unify. Since this task requires to capture the visual details of the image, the unified model takes advantage from its learned visual details generation capability. As demonstrated, our method brings improvement to base model in many subtasks. For the tool-augmented VLMs, without such auxiliary images, their performance will drop significantly. In contrast, our model, equipped with latent reasoning capability, does not depend on external tools. By generating latent visual tokens, the model conducts visual search intrinsically rather than relying on auxiliary tools, resulting in stronger robustness and better overall performance.

By comparing the performance of our methods using SFT and RL, we can see that RL is more effective in improving the vision-intensive perception tasks than reasoning tasks. The reason is that the perception tasks typically require better fine-grained understanding of the image input, which needs the effective coordination between visual embedding and text token generation. However, RL leads to a significant degradation in the two dimensions from LogicVista benchmark. We observe that the two subtasks require to handle abstract logical patterns and the CoT output tends to be lengthy. A possible reason is that the long output pattern has not been well captured by the RL training data.

### 5.3 FURTHER ANALYSIS

**Ablation Study.** In our method, the latent visual embeddings within the modal-mixed CoT and the diffusion model based decoder are two key components. To study the effectiveness of these parts, we devise two variant models: (1) **Text-only Training** that only uses the text parts of the annotated CoT for training; (2) **Similarity Loss** that replaces the diffusion model based decoder by a MLP head, and directly uses the cosine similarity loss for optimizing the projected LLM output (Yang et al., 2025b). We conduct the experiments on both the vision-intensive perception and reasoning datasets, *i.e.*, six subtasks from V\* benchmark, MME-Unify and LogicVista. As shown in Table 3, our method consistently outperforms both the variant models and the base model on average. It indicates the effectiveness of both the latent embedding based modal-mixed CoT and the diffusion model based decoder. Among all the compared methods, the better results of the Similarity Loss model, together with our own method, demonstrate the effectiveness of latent-text interleaved reasoning. Moreover, the performance gap between our method and the Similarity Loss model highlights the importance of the diffusion decoder. By explicitly modeling the distribution of latent visual embeddings, the diffusion model based decoder enables the generation of higher-quality visual tokens, which serve as more informative and structured visual rationales, thereby enhancing reasoning capability.

**Catastrophic Forgetting Study.** In our approach, we use the visual encoder and connection layer from the VLM itself to supervise the training of our latent reasoning capability, and adopt a diffusion-based decoder for decomposing the high-level and low-level vision generation abilities. Such a well-aligned objective can avoid the catastrophic forgetting of the VLM for its original language-based reasoning ability. To study it, we remove the latent reasoning related modules (*i.e.*, diffusion model based decoder and special tokens), and use the VLM fine-tuned by our method for performing language-based CoT reasoning. The results in Table 4 shows that our model’s language-based CoT



Table 4: Ability forgetting study results testing whether our fine-tuned VLM maintains the original language-only CoT reasoning capability. **Qwen2.5-VL** denotes the baseline model Qwen2.5-VL-7B-Instruct.

Model	MME-Unify		LogicVista		Average
	Spot Diff.	Aux. Lines	Ind.	Spat.	
<b>Qwen2.5-VL</b>	13.0	<u>32.7</u>	<u>25.2</u>	19.0	<u>22.5</u>
<b>Ours (SFT)</b>	<b>27.0</b>	<b>34.6</b>	<b>28.0</b>	<b>27.9</b>	<b>29.4</b>
<b>Language-only</b>	<u>18.0</u>	25.0	22.1	<u>21.5</u>	21.6

Table 5: Controlled efficiency comparison on a single H100 GPU. We compare 32 steps of text/latent generation against a single tool-use invocation in Thyme.

Method	Scope	Latency (s)
<b>Qwen2.5-VL</b>	32 Tokens	1.0311
<b>Thyme</b>	Single Tool Call	8.3575
<b>Ours (Latent-token)</b>	32 Latent Steps	3.1001

reasoning capability has not been hurt a lot, with comparable performance with the backbone model. It demonstrates that our method can well keep the original knowledge and capability of the VLM, and also empowers it with a new modal-mixed CoT reasoning ability involving latent visual embeddings.

**Efficiency Study.** To isolate the true computational overhead of our latent mechanism, we conduct a controlled analysis comparing three distinct reasoning paradigms under identical hardware conditions (NVIDIA H100 GPU). Specifically, we evaluate: (1) **Text-only generation** of 32 tokens; (2) **Thyme**Zhang et al. (2025), a representative VLM variant based on Qwen2.5-VL-7B-Instruct that performs visual reasoning via a single tool-use invocation (generating Python code, executing image edits, and re-encoding); and (3) Our **Latent-token generation** of 32 steps (with 50 denoising steps). The results are summarized in Table 5. We observe that a single tool-use cycle in Thyme incurs a significant latency of 8.36s. A detailed breakdown reveals that while the CPU-based tool execution is negligible ( $\sim 0.02$ s), the process is bottlenecked by expensive GPU forward passes: specifically, autoregressive code generation ( $\sim 8.3$ s) and image re-encoding ( $\sim 0.2$ s). In contrast, our latent reasoning operates directly within the embedding space, bypassing these external loops. It requires approximately 0.10s per step, totaling only 3.10s for a sequence of 32 steps—making it more efficient than tool-based paradigms.

**Hyper-parameter Tuning.** A key component of our training objective is the hyperparameter  $\lambda$  which balances textual next-token prediction and latent diffusion supervision. To understand the impact of this hyperparameter, we conducted an ablation study with  $\lambda$  set to 0.1, 1.0, and 10. The results are presented in Table 6. A small  $\lambda$  of 0.1 achieves the highest score on the attribute task  $V^*$  benchmark, but for spatial task of LogicVista have low score. Increasing  $\lambda$  to 1.0 slight decrease in performance on the attribute and inductive tasks, it dramatically boosts performance on complex spatial reasoning. The spatial task of LogicVista score increases to 31.6. However, increasing the weight further to  $\lambda = 10$  proves to be detrimental. It significantly degrades performance across nearly all other metrics, we hypothesize that large  $\lambda$  forces the model to focus too heavily on the visual latent embeddings, potentially makes reasoning performance drop. Based on this analysis, we selected  $\lambda = 1.0$  for all our main experiments.

**Ablation Study on Latent Token Budget** To analyze the impact of the latent token budget, we conducted an ablation study on the  $V^*$  benchmark, specifically evaluating the *Attribute (Attr)* and *Spatial* subsets. We varied the number of latent tokens from 4 to 128 to observe the performance trends, as summarized in Table 7. The *Spatial* subset exhibits significant sensitivity to the token budget, showing an “inverted-U” trend where performance improves with more tokens, peaking at 64 tokens (80.3), before declining at 128. In contrast, the *Attr* subset remains relatively stable across all configurations, with scores fluctuating between approximately 79 and 83. This suggests that while

Table 6: Hyperparameter tuning results of our method with different values of  $\lambda$ .

$\lambda$	V* Benchmark		LogicVista		Average
	Attr	Spatial	Ind.	Spat.	
<b>0.1</b>	<b>85.3</b>	77.6	<b>30.1</b>	15.2	<u>52.1</u>
<b>1.0</b>	<u>80.2</u>	<u>78.9</u>	<u>28.0</u>	<b>31.6</b>	<b>54.7</b>
<b>10</b>	75.9	<b>80.3</b>	25.7	<u>20.3</u>	50.6

Table 7: Ablation study on the number of latent tokens on the V\* benchmark.

Latent Tokens	Attr	Spatial	Overall
<b>4</b>	81.9	68.4	75.2
<b>8</b>	<b>82.8</b>	73.7	<u>78.3</u>
<b>16</b>	81.0	69.7	<u>75.4</u>
<b>32</b>	80.2	<u>78.9</u>	79.6
<b>64</b>	<u>79.3</u>	<b>80.3</b>	<b>79.8</b>
<b>128</b>	<u>79.3</u>	69.7	74.5

basic attributes can be captured with fewer tokens, complex spatial relationships benefit from a larger latent representation.

Table 8: Performance comparison on Qwen3-VL-4B-Instruct.

Model	V* Benchmark		LogicVista		MMIQ		
	Attr	Spatial	Ind.	Spat.	Math	Log.	2D.
<b>Qwen3-VL</b>	<u>41.7</u>	<u>35.5</u>	<u>15.0</u>	<u>16.4</u>	<b>22.6</b>	<u>23.2</u>	<u>22.2</u>
<b>Ours</b>	<b>76.7</b>	<b>77.6</b>	<b>27.4</b>	<b>25.3</b>	<u>21.6</u>	<b>25.1</b>	<b>29.8</b>

**Generalization on Different Base Models.** To investigate the generalizability of our method across different model architectures and parameter scales, we extended our experiments to the Qwen3-VL-4B-Instruct Bai et al. (2025a). As shown in Table 8, our method consistently outperforms the baseline Qwen3-VL-4B-Instruct across various benchmarks, including V\*, Logicvista, and MMIQ. Notably, we observe substantial gains in attribute and spatial reasoning tasks (V\*) and logic induction (Logicvista). These results demonstrate that our approach is effective and scalable, capable of generalizing to newer model architectures.

## 6 CONCLUSION

In this paper, we presented modal-mixed chain-of-thought (CoT), a new reasoning paradigm that enables a VLM to interleave language with compact visual “sketches” encoded as latent embeddings. To make these latents usable without eroding the original knowledge and capability of the VLM, we proposed to (1) train the VLM to reconstruct its own produced vision embeddings for intermediate images, and (2) attach a diffusion-based latent decoder that shoulders fine-grained perceptual detail while the language backbone supplies high-level intent. Based on the above architecture, we devised a two-stage training recipe, that first performs supervised fine-tuning with a joint next-token and latent objective then followed by reinforcement learning. Extensive experiments have demonstrated the effectiveness of our method on 11 multimodal tasks. In the future, we will extend our method to other modalities such as audio and 3D, for devising a unified paradigm.

## REFERENCES

Jean-Baptiste Alayrac, Jeff Donahue, Pauline Luc, Antoine Miech, Iain Barr, Yana Hasson, Karel Lenc, Arthur Mensch, Katherine Millican, Malcolm Reynolds, et al. Flamingo: a visual language model for few-shot learning. *Advances in neural information processing systems*, 35:23716–23736, 2022.

- 
- Shuai Bai, Yuxuan Cai, Ruizhe Chen, Keqin Chen, Xionghui Chen, Zesen Cheng, Lianghao Deng, Wei Ding, Chang Gao, Chunjiang Ge, Wenbin Ge, Zhifang Guo, Qidong Huang, Jie Huang, Fei Huang, Binyuan Hui, Shutong Jiang, Zhaohai Li, Mingsheng Li, Mei Li, Kaixin Li, Zicheng Lin, Junyang Lin, Xuejing Liu, Jiawei Liu, Chenglong Liu, Yang Liu, Dayiheng Liu, Shixuan Liu, Dunjie Lu, Ruilin Luo, Chenxu Lv, Rui Men, Lingchen Meng, Xuancheng Ren, Xingzhang Ren, Sibao Song, Yuchong Sun, Jun Tang, Jianhong Tu, Jianqiang Wan, Peng Wang, Pengfei Wang, Qiuyue Wang, Yuxuan Wang, Tianbao Xie, Yiheng Xu, Haiyang Xu, Jin Xu, Zhibo Yang, Mingkun Yang, Jianxin Yang, An Yang, Bowen Yu, Fei Zhang, Hang Zhang, Xi Zhang, Bo Zheng, Humen Zhong, Jingren Zhou, Fan Zhou, Jing Zhou, Yuanzhi Zhu, and Ke Zhu. Qwen3-vl technical report, 2025a. URL <https://arxiv.org/abs/2511.21631>.
- Shuai Bai, Keqin Chen, Xuejing Liu, Jialin Wang, Wenbin Ge, Sibao Song, Kai Dang, Peng Wang, Shijie Wang, Jun Tang, et al. Qwen2. 5-vl technical report. *arXiv preprint arXiv:2502.13923*, 2025b.
- Loïc Barrault, Paul-Ambroise Duquenne, Maha Elbayad, Artyom Kozhevnikov, Belen Alastruey, Pierre Andrews, Mariano Coria, Guillaume Couairon, Marta R Costa-jussà, David Dale, et al. Large concept models: Language modeling in a sentence representation space. *arXiv preprint arXiv:2412.08821*, 2024.
- Huanqia Cai, Yijun Yang, and Winston Hu. Mm-iq: Benchmarking human-like abstraction and reasoning in multimodal models. *arXiv preprint arXiv:2502.00698*, 2025.
- Xu Cao, Bolin Lai, Wenqian Ye, Yunsheng Ma, Joerg Heintz, Jintai Chen, Jianguo Cao, and James M Rehg. What is the visual cognition gap between humans and multimodal llms? *arXiv preprint arXiv:2406.10424*, 2024.
- Shiqi Chen, Tongyao Zhu, Ruochen Zhou, Jinghan Zhang, Siyang Gao, Juan Carlos Niebles, Mor Geva, Junxian He, Jiajun Wu, and Manling Li. Why is spatial reasoning hard for vlms? an attention mechanism perspective on focus areas, 2025a. URL <https://arxiv.org/abs/2503.01773>.
- Xiaokang Chen, Zhiyu Wu, Xingchao Liu, Zizheng Pan, Wen Liu, Zhenda Xie, Xingkai Yu, and Chong Ruan. Janus-pro: Unified multimodal understanding and generation with data and model scaling. *arXiv preprint arXiv:2501.17811*, 2025b.
- Yan Chen, Long Li, Teng Xi, Long Zeng, and Jingdong Wang. Perception before reasoning: Two-stage reinforcement learning for visual reasoning in vision-language models, 2025c. URL <https://arxiv.org/abs/2509.13031>.
- Yangyi Chen, Karan Sikka, Michael Cogswell, Heng Ji, and Ajay Divakaran. Measuring and improving chain-of-thought reasoning in vision-language models, 2024a. URL <https://arxiv.org/abs/2309.04461>.
- Zhe Chen, Weiyun Wang, Yue Cao, Yangzhou Liu, Zhangwei Gao, Erfei Cui, Jinguo Zhu, Shenglong Ye, Hao Tian, Zhaoyang Liu, et al. Expanding performance boundaries of open-source multimodal models with model, data, and test-time scaling. *arXiv preprint arXiv:2412.05271*, 2024b.
- Zhenfang Chen, Qinlong Zhou, Yikang Shen, Yining Hong, Zhiqing Sun, Dan Gutfreund, and Chuang Gan. Visual chain-of-thought prompting for knowledge-based visual reasoning. *arXiv preprint arXiv:2301.05226*, 2023.
- Yuntian Deng, Kiran Prasad, Roland Fernandez, Paul Smolensky, Vishrav Chaudhary, and Stuart Shieber. Implicit chain of thought reasoning via knowledge distillation. *arXiv preprint arXiv:2311.01460*, 2023.
- Yuntian Deng, Yejin Choi, and Stuart Shieber. From explicit cot to implicit cot: Learning to internalize cot step by step. *arXiv preprint arXiv:2405.14838*, 2024.
- Alexey Dosovitskiy, Lucas Beyer, Alexander Kolesnikov, Dirk Weissenborn, Xiaohua Zhai, Thomas Unterthiner, Mostafa Dehghani, Matthias Minderer, Georg Heigold, Sylvain Gelly, et al. An image is worth 16x16 words: Transformers for image recognition at scale. *arXiv preprint arXiv:2010.11929*, 2020.

- 
- Ying Fan, Yilun Du, Kannan Ramchandran, and Kangwook Lee. Looped transformers for length generalization. *arXiv preprint arXiv:2409.15647*, 2024.
- Jun Gao, Yongqi Li, Ziqiang Cao, and Wenjie Li. Interleaved-modal chain-of-thought, 2025. URL <https://arxiv.org/abs/2411.19488>.
- Angeliki Giannou, Shashank Rajput, Jy-yong Sohn, Kangwook Lee, Jason D Lee, and Dimitris Papailiopoulos. Looped transformers as programmable computers. In *International Conference on Machine Learning*, pp. 11398–11442. PMLR, 2023.
- Sachin Goyal, Ziwei Ji, Ankit Singh Rawat, Aditya Krishna Menon, Sanjiv Kumar, and Vaishnavh Nagarajan. Think before you speak: Training language models with pause tokens. *arXiv preprint arXiv:2310.02226*, 2023.
- Daya Guo, Dejian Yang, Haowei Zhang, Junxiao Song, Ruoyu Zhang, Runxin Xu, Qihao Zhu, Shirong Ma, Peiyi Wang, Xiao Bi, et al. Deepseek-r1: Incentivizing reasoning capability in llms via reinforcement learning. *arXiv preprint arXiv:2501.12948*, 2025.
- Shibo Hao, Yi Gu, Haotian Luo, Tianyang Liu, Xiyang Shao, Xinyuan Wang, Shuhua Xie, Haodi Ma, Adithya Samavedhi, Qiyue Gao, et al. Llm reasoners: New evaluation, library, and analysis of step-by-step reasoning with large language models. *arXiv preprint arXiv:2404.05221*, 2024a.
- Shibo Hao, Sainbayar Sukhbaatar, DiJia Su, Xian Li, Zhiting Hu, Jason Weston, and Yuandong Tian. Training large language models to reason in a continuous latent space. *arXiv preprint arXiv:2412.06769*, 2024b.
- Alex Havrilla, Yuqing Du, Sharath Chandra Raparthy, Christoforos Nalmpantis, Jane Dwivedi-Yu, Maksym Zhuravinskiy, Eric Hambro, Sainbayar Sukhbaatar, and Roberta Raileanu. Teaching large language models to reason with reinforcement learning. *arXiv preprint arXiv:2403.04642*, 2024.
- Aaron Jaech, Adam Kalai, Adam Lerer, Adam Richardson, Ahmed El-Kishky, Aiden Low, Alec Helyar, Aleksander Madry, Alex Beutel, Alex Carney, et al. Openai o1 system card. *arXiv preprint arXiv:2412.16720*, 2024.
- Tushar Khot, Harsh Trivedi, Matthew Finlayson, Yao Fu, Kyle Richardson, Peter Clark, and Ashish Sabharwal. Decomposed prompting: A modular approach for solving complex tasks. *arXiv preprint arXiv:2210.02406*, 2022.
- Ang Li, Charles Wang, Kaiyu Yue, Zikui Cai, Ollie Liu, Deqing Fu, Peng Guo, Wang Bill Zhu, Vatsal Sharan, Robin Jia, Willie Neiswanger, Furong Huang, Tom Goldstein, and Micah Goldblum. Zebra-cot: A dataset for interleaved vision language reasoning, 2025a. URL <https://arxiv.org/abs/2507.16746>.
- Chengzu Li, Wenshan Wu, Huanyu Zhang, Yan Xia, Shaoguang Mao, Li Dong, Ivan Vulić, and Furu Wei. Imagine while reasoning in space: Multimodal visualization-of-thought. *arXiv preprint arXiv:2501.07542*, 2025b.
- Junnan Li, Dongxu Li, Silvio Savarese, and Steven Hoi. Blip-2: Bootstrapping language-image pre-training with frozen image encoders and large language models. In *International conference on machine learning*, pp. 19730–19742. PMLR, 2023.
- Haotian Liu, Chunyuan Li, Qingyang Wu, and Yong Jae Lee. Visual instruction tuning. *Advances in neural information processing systems*, 36:34892–34916, 2023a.
- Haotian Liu, Chunyuan Li, Qingyang Wu, and Yong Jae Lee. Visual instruction tuning, 2023b. URL <https://arxiv.org/abs/2304.08485>.
- Haotian Liu, Chunyuan Li, Yuheng Li, and Yong Jae Lee. Improved baselines with visual instruction tuning. In *Proceedings of the IEEE/CVF conference on computer vision and pattern recognition*, pp. 26296–26306, 2024.
- Fanqing Meng, Lingxiao Du, Zongkai Liu, Zhixiang Zhou, Quanfeng Lu, Daocheng Fu, Tiancheng Han, Botian Shi, Wenhai Wang, Junjun He, et al. Mm-eureka: Exploring the frontiers of multimodal reasoning with rule-based reinforcement learning. *arXiv preprint arXiv:2503.07365*, 2025.

- 
- Zhiliang Peng, Wenhui Wang, Li Dong, Yaru Hao, Shaohan Huang, Shuming Ma, and Furu Wei. Kosmos-2: Grounding multimodal large language models to the world. *arXiv preprint arXiv:2306.14824*, 2023.
- Jacob Pfau, William Merrill, and Samuel R Bowman. Let’s think dot by dot: Hidden computation in transformer language models. *arXiv preprint arXiv:2404.15758*, 2024.
- Zenon W Pylyshyn. Mental imagery: In search of a theory. *Behavioral and brain sciences*, 25(2): 157–182, 2002.
- Alan Richardson. *Mental imagery*. Springer, 2013.
- Robin Rombach, Andreas Blattmann, Dominik Lorenz, Patrick Esser, and Björn Ommer. High-resolution image synthesis with latent diffusion models, 2022. URL <https://arxiv.org/abs/2112.10752>.
- Zhihong Shao, Peiyi Wang, Qihao Zhu, Runxin Xu, Junxiao Song, Xiao Bi, Haowei Zhang, Mingchuan Zhang, YK Li, Yang Wu, et al. Deepseekmath: Pushing the limits of mathematical reasoning in open language models. *arXiv preprint arXiv:2402.03300*, 2024.
- Peiyi Wang, Lei Li, Zhihong Shao, Runxin Xu, Damai Dai, Yifei Li, Deli Chen, Yu Wu, and Zhifang Sui. Math-shepherd: Verify and reinforce llms step-by-step without human annotations. In *Proceedings of the 62nd Annual Meeting of the Association for Computational Linguistics (Volume 1: Long Papers)*, pp. 9426–9439, 2024.
- Yikun Wang, Siyin Wang, Qinyuan Cheng, Zhaoye Fei, Liang Ding, Qipeng Guo, Dacheng Tao, and Xipeng Qiu. Visuothink: Empowering lvm reasoning with multimodal tree search, 2025a. URL <https://arxiv.org/abs/2504.09130>.
- Yuqi Wang, Xinghang Li, Wenxuan Wang, Junbo Zhang, Yingyan Li, Yuntao Chen, Xinlong Wang, and Zhaoxiang Zhang. Unified vision-language-action model, 2025b. URL <https://arxiv.org/abs/2506.19850>.
- Jason Wei, Xuezhi Wang, Dale Schuurmans, Maarten Bosma, Fei Xia, Ed Chi, Quoc V Le, Denny Zhou, et al. Chain-of-thought prompting elicits reasoning in large language models. *Advances in neural information processing systems*, 35:24824–24837, 2022.
- Penghao Wu and Saining Xie. V?: Guided visual search as a core mechanism in multimodal llms. In *Proceedings of the IEEE/CVF Conference on Computer Vision and Pattern Recognition*, pp. 13084–13094, 2024.
- Wenyi Wu, Zixuan Song, Kun Zhou, Yifei Shao, Zhiting Hu, and Biwei Huang. Towards general continuous memory for vision-language models. *arXiv preprint arXiv:2505.17670*, 2025.
- Yijia Xiao, Edward Sun, Tianyu Liu, and Wei Wang. Logicvista: Multimodal llm logical reasoning benchmark in visual contexts. *arXiv preprint arXiv:2407.04973*, 2024.
- Wulin Xie, Yi-Fan Zhang, Chaoyou Fu, Yang Shi, Bingyan Nie, Hongkai Chen, Zhang Zhang, Liang Wang, and Tieniu Tan. Mme-unify: A comprehensive benchmark for unified multimodal understanding and generation models. *arXiv preprint arXiv:2504.03641*, 2025.
- Yuxi Xie, Kenji Kawaguchi, Yiran Zhao, James Xu Zhao, Min-Yen Kan, Junxian He, and Michael Xie. Self-evaluation guided beam search for reasoning. *Advances in Neural Information Processing Systems*, 36, 2023.
- Weiyue Xu, Jiahao Wang, Weiyun Wang, Zhe Chen, Wengang Zhou, Aijun Yang, Lewei Lu, Houqiang Li, Xiaohua Wang, Xizhou Zhu, Wenhai Wang, Jifeng Dai, and Jinguo Zhu. Visulogic: A benchmark for evaluating visual reasoning in multi-modal large language models. *arXiv preprint arXiv:2504.15279*, 2025. URL <https://arxiv.org/abs/2504.15279>.
- Yi Yang, Xiaoxuan He, Hongkun Pan, Xiyan Jiang, Yan Deng, Xingtao Yang, Haoyu Lu, Dacheng Yin, Fengyun Rao, Minfeng Zhu, et al. R1-onevision: Advancing generalized multimodal reasoning through cross-modal formalization. *arXiv preprint arXiv:2503.10615*, 2025a.

- 
- Zeyuan Yang, Xueyang Yu, Delin Chen, Maohao Shen, and Chuang Gan. Machine mental imagery: Empower multimodal reasoning with latent visual tokens. *arXiv preprint arXiv:2506.17218*, 2025b.
- Shunyu Yao, Dian Yu, Jeffrey Zhao, Izhak Shafran, Tom Griffiths, Yuan Cao, and Karthik Narasimhan. Tree of thoughts: Deliberate problem solving with large language models. *Advances in Neural Information Processing Systems*, 36, 2023.
- Chao Yi, Yu-Hang He, De-Chuan Zhan, and Han-Jia Ye. Bridge the modality and capability gaps in vision-language model selection, 2025. URL <https://arxiv.org/abs/2403.13797>.
- Longhui Yu, Weisen Jiang, Han Shi, Jincheng Yu, Zhengying Liu, Yu Zhang, James T Kwok, Zhenguo Li, Adrian Weller, and Weiyang Liu. Metamath: Bootstrap your own mathematical questions for large language models. *arXiv preprint arXiv:2309.12284*, 2023.
- Ping Yu, Jing Xu, Jason Weston, and Ilia Kulikov. Distilling system 2 into system 1. *arXiv preprint arXiv:2407.06023*, 2024.
- Xiang Yue, Xingwei Qu, Ge Zhang, Yao Fu, Wenhao Huang, Huan Sun, Yu Su, and Wenhui Chen. Mammoth: Building math generalist models through hybrid instruction tuning. *arXiv preprint arXiv:2309.05653*, 2023.
- Chi Zhang, Feng Gao, Baoxiong Jia, Yixin Zhu, and Song-Chun Zhu. Raven: A dataset for relational and analogical visual reasoning. In *Proceedings of the IEEE Conference on Computer Vision and Pattern Recognition (CVPR)*, 2019.
- Yi-Fan Zhang, Xingyu Lu, Shukang Yin, Chaoyou Fu, Wei Chen, Xiao Hu, Bin Wen, Kaiyu Jiang, Changyi Liu, Tianke Zhang, et al. Thyme: Think beyond images. *arXiv preprint arXiv:2508.11630*, 2025.
- Zhuosheng Zhang, Aston Zhang, Mu Li, Hai Zhao, George Karypis, and Alex Smola. Multimodal chain-of-thought reasoning in language models, 2024. URL <https://arxiv.org/abs/2302.00923>.
- Denny Zhou, Nathanael Schärli, Le Hou, Jason Wei, Nathan Scales, Xuezhi Wang, Dale Schuurmans, Claire Cui, Olivier Bousquet, Quoc Le, et al. Least-to-most prompting enables complex reasoning in large language models. *arXiv preprint arXiv:2205.10625*, 2022.
- Chenming Zhu, Tai Wang, Wenwei Zhang, Kai Chen, and Xihui Liu. Scanreason: Empowering 3d visual grounding with reasoning capabilities, 2024. URL <https://arxiv.org/abs/2407.01525>.
- Hanlin Zhu, Shibo Hao, Zhiting Hu, Jiantao Jiao, Stuart Russell, and Yuandong Tian. Reasoning by superposition: A theoretical perspective on chain of continuous thought. *arXiv preprint arXiv:2505.12514*, 2025.

## A VISUALIZATION RESULTS

To demonstrate that the generated visual tokens truly contribute to the model’s reasoning in visual search, we extract all attention maps associated with the 32 visual tokens at an intermediate layer (Layer 14) and average them. The resulting attention heatmap is shown in Figure 2.



**Question ID: 7**

**Q: What is the color of the Apple logo?**

(A) polychromatic (B) red (C) white (D) silver

**Label: A**



**Question ID: 17**

**Q: What is the color of the bicycle?**

(A) blue (B) white (C) silver (D) red

**Label: D**

Figure 2: **Visualization of Visual Tokens Attention.** The heatmaps (Layer 14) are shown above their respective QA pairs. The model successfully focuses on the semantic regions relevant to the question.

---

## B QUALITATIVE ANALYSIS OF LATENT REASONING

We provide qualitative examples comparing the reasoning process of our model against Qwen. Our model utilizes generated visual tokens (represented as `<|latent_start|>` sequences) to explicitly “visualize” intermediate steps, leading to more accurate answers.



**Question:** What is the color of the woman’s shirt?

(A) white (B) purple (C) blue (D) pink

Answer with the option’s letter from the given choices directly.

**Ours:**

`<think>` To determine the woman’s shirt color, I need to locate her within the image and observe her attire. The woman is swinging on a rope from a treehouse. To accurately identify her shirt color, I will generate a zoomed-in view of her upper body.

`<|latent_start|><|latent_pad|>...<|latent_pad|>`

The zoomed-in image clearly shows the woman wearing a purple top. Based on this clear visual evidence, the color of her shirt can be definitively identified. `</think>`

**Final Answer: B ✓ (Correct)**

**Qwen2.5-VL-7B-Instruct:**

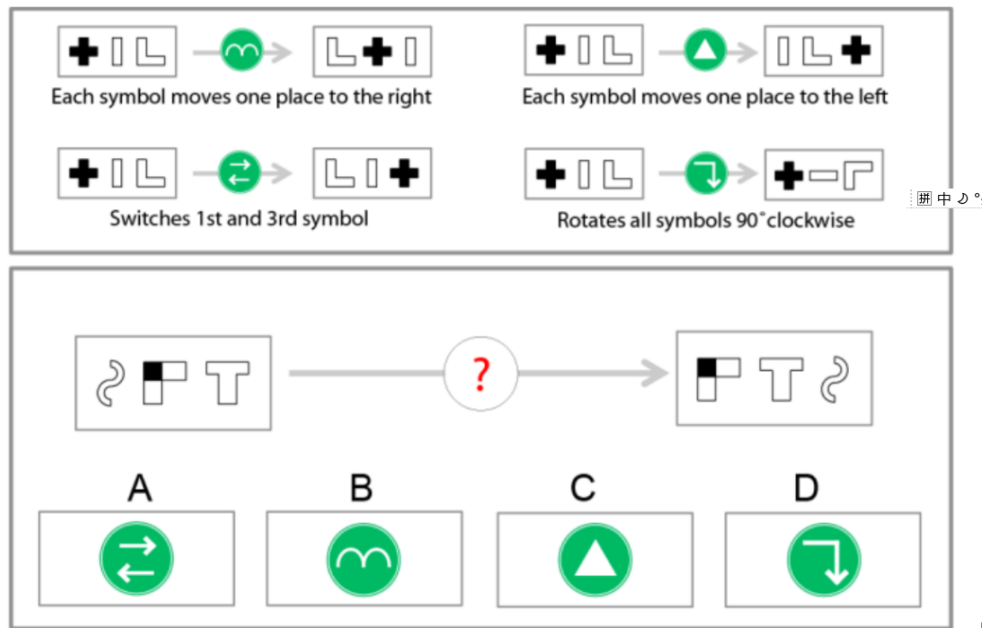
`<think>` The question asks for the color of the woman’s shirt. Observing the image, the woman appears to be wearing a shirt that is a shade of purple. The other options (pink, blue, and white) do not match the visible color of the shirt in the image. Therefore, the correct answer is A. `</think>`

**A. The color of the woman’s shirt is purple. ✗ (Incorrect - Hallucination)**

(Note: Qwen correctly identifies the color as purple but hallucinates that option A corresponds to purple, whereas A is white.)

Figure 3: **Case Study 1: Fine-grained Attribute Recognition.** Our model generates visual tokens to focus on the person, correctly mapping the visual attribute to Option B. The baseline model suffers from hallucination between the visual perception and the option selection.



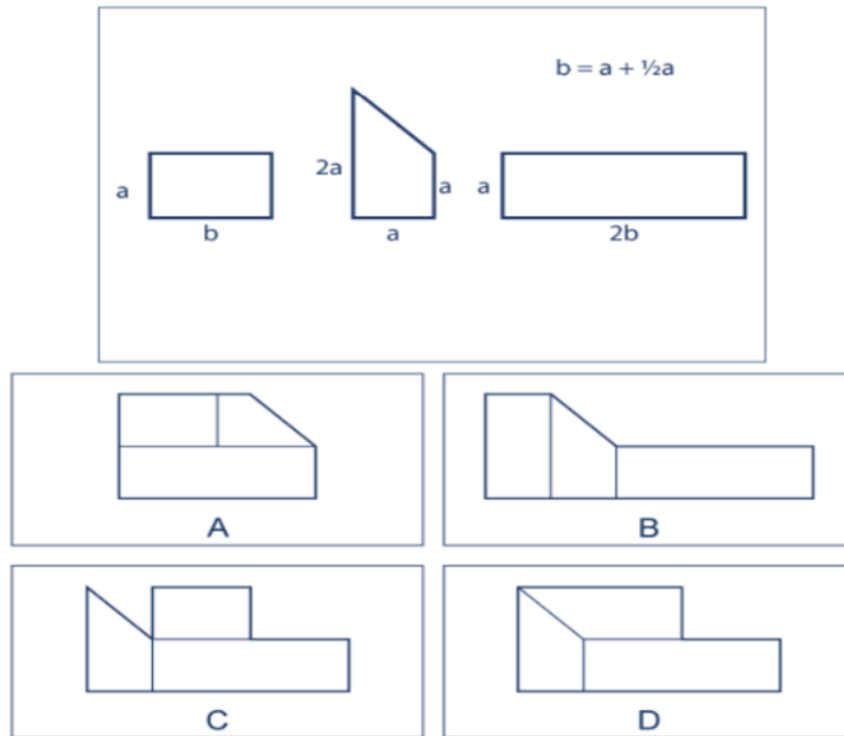


**Task:** Identify the missing operation in the transformation sequence.

**Ours:**  
 The problem presents a sequence of transformations applied to a set of symbols. I need to identify the pattern governing these transformations to determine the missing element. Let's analyze the initial configuration of symbols and the transformation steps shown in the problem image. The first step is to visualize the result of the first operation.  
 <|latent\_start|><|latent\_pad|>...<|latent\_pad|>  
 The visual thought shows the result after the first operation, which appears to be a rotation. Now, let's visualize the next step in the sequence.  
 <|latent\_start|><|latent\_pad|>...<|latent\_pad|>  
 This visual thought represents the state after the second operation. Observing the sequence of operations and their effects on the symbols, the third operation is a rotation. The fourth operation involves swapping the first and third symbols.  
 <|latent\_start|><|latent\_pad|>...<|latent\_pad|>  
 This final visual thought shows the outcome of all four operations. Comparing this resulting configuration with the provided options, option C matches the sequence of transformations performed.  
**Final Answer: C ✓**

**Qwen2.5-VL-7B-Instruct:**  
 <think> To solve this, let's analyze each transformation given and apply it to the original sequence: [...] C: This option shows a leftward-pointing triangle, which doesn't seem to represent any of the operations described. D: This option shows a rightward-pointing arrow, matching the action of moving symbols one place to the right. Considering the information given, the operation that matches moving symbols one place to the right is represented by the rightward arrow. </think>  
**Final Answer: D ✗**

Figure 4: **Case Study 2: Abstract Logic Reasoning.** Our model explicitly visualizes the state of symbols after each transformation step using latent visual tokens, enabling it to track the multi-step logic correctly.



**Task:** Identify which shape can be formed using the given single piece.

**Ours:**

The problem asks to identify which of the provided options can be created using the single piece shown in the diagram. To determine the correct option, I will visualize how the piece fits into each potential shape.

<|latent\_start|><|latent\_pad|>...<|latent\_pad|>

Placing the piece into option A shows that it does not fit correctly; there is a gap on the left side.

<|latent\_start|><|latent\_pad|>...<|latent\_pad|>

Placing the piece into option B reveals that it also does not fit properly, leaving gaps or overlapping. When placing the piece into option C, it appears to fit perfectly, completing the shape without gaps or overlaps.

<|latent\_start|><|latent\_pad|>...<|latent\_pad|>

Testing option D shows that this piece does not match the required shape for a seamless fit. Based on the visual fitting, only option C allows the piece to complete the figure seamlessly.

**Final Answer: C ✓**

**Qwen2.5-VL-7B-Instruct:**

<think> [...] B. This figure seems to fit the components correctly. It includes a right triangle with legs 'a' and 'b', which can be rearranged to form the original shape. Additionally, there is a square that matches the size 'a' perfectly. [...] After careful analysis, we can conclude that figure B is the one that can be formed using the given piece. </think>

**Final Answer: B ✗**

Figure 5: **Case Study 3: Spatial Fitting.** By mentally "placing" the piece into the options via latent visualization, our model correctly identifies the geometric correspondence, whereas the baseline relies on erroneous textual descriptions of the shapes.